Proceedings of IDETC/CIE 2005
ASME 2005 International Design Engineering Technical Conferences
& Computers and Information in Engineering Conference
September 24-28, 2005, Long Beach, California USA

DETC2005-84822

NONLINEAR DYNAMIC ANALYSIS AND CHAOTIC BEHAVIOR IN ATOMIC FORCE MICROSCOPY

Hossein Nejat Pishkenari [1], Nader Jalili [2], Aria Alasty [1] and Ali Meghdari [1]

[1] Center of Excellence in Design, Robotics and Automation (CEDRA), School of Mechanical Engineering, Sharif University of Technology, Tehran, Iran.

[2] Smart Structure and NanoElectroMechanical Systems Laboratory, Department of Mechanical Engineering, Clemson University, Clemson, South Carolina 29634-0921, USA (Jalili@clemson.edu).

ABSTRACT

The atomic force microscope (AFM) system has evolved into a useful tool for direct measurements of intermolecular forces with atomic-resolution characterization that can be employed in a broad spectrum of applications. In this paper, the nonlinear dynamical behavior of the AFM is studied. This is achieved by modeling the microcantilever as a single mode approximation (lumped-parameters model) and considering the interaction between the sample and cantilever in the form of van der Waals potential. The resultant nonlinear system is then analyzed using Melnikov method, which predicts the regions in which only periodic and quasi-periodic motions exist, and also predicts the regions that chaotic motion is possible. Numerical simulations are used to verify the presence of such chaotic invariant sets determined by Melnikov theory. Finally, the amplitude of vibration in which chaos is appeared is investigated and such irregular motion is proven by several methods including Poincare maps, Fourier transform, autocorrelation function and Lyapunov exponents.

INTRODUCTION

The atomic force microscope (AFM) system has evolved into a useful tool for direct measurements of intermolecular forces with atomic-resolution characterization that can be employed in a broad spectrum of applications such as electronics, semi-conductors, manufacturing, polymers, biological analysis, and biomaterials [1]. Specifically, AFM-based systems provide additional capabilities and advantageous relative to other microscopic methods (e.g., scanning electron microscopy (SEM) and transmission electron microscopy (TEM)) with regard to studies of metallic surfaces and microstructures by providing reliable measurements at the nanometer scale [2-4]. AFM can also be used for nano-indentation to provide in situ imaging ability without moving the sample, switching tips, relocating the area for scanning, or using an entirely different instrument to image the indentation [5-7]. Assembly of nanoparticles and linking them to electrical leads, such as random deposition of clusters between electrodes [8], binding by wet chemistry [9], and electrostatic trapping [10], all serve as other important applications of the AFM technique. A typical AFM system consists of a micro-cantilever probe with a sharp tip mounted to a piezoelectric actuator with a position sensitive photo detector receiving a laser beam reflected off the end-point of the beam to provide cantilever deflection feedback (refer to Fig. 1), [11].

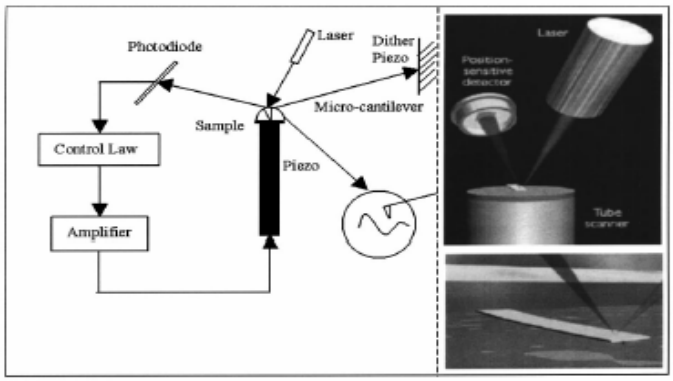

Fig. 1 (Left) Schematic depicting basic AFM operation and sub-components, and (right) real scale drawing (from [11]).

Though widely practiced, open-loop operation for i) noncontact modes, ii) tapping modes, and iii) contact modes exhibit the potential for chaotic behavior in the cantilever tip displacement thus rendering erroneous topographical

information. As a result, recent research on AFM systems has focused on detailed numerical analysis such that this chaotic behavior region can be well defined and ideally avoided. For example, a harmonic balancing and averaging technique is used to predict the behavior of the cantilever during tapping mode operation [12]. In addition, the Lennard-Jones potential within the dynamics for the AFM system has been utilized such that the chaotic region of operation could be determined [13]. In addition to analytical methodology, several feedback control strategies have been developed in order to improve the AFM region of operation. The Melnikov method has been utilized to analyze a simple model for the possibility of chaotic motion [14]. A feedback linearization and singular perturbation techniques have been used to design an output, high-gain feedback sample surface tracking controller [11, 15-16].

ATOMIC FORCE MICROSCOPY MODELING

The AFM is modeled through a lumped-parameters system approach as shown in Figure 2. The cantilever is modeled as a spring–mass system which is excited harmonically by the motion of the spring base. The dynamics for this system can be represented in the following form [1, 11].

$$m_e \ddot{x}(t) + b(\dot{x}(t) - \dot{d}(t)) + k(x(t) - d(t)) = f_{IL}(t) \qquad (1)$$

where $d(t)$ and $x(t)$ denote the base motion and the cantilever tip displacement relative to the fixed base frame, respectively, m_e, b and k denote the cantilever tip mass, damping coefficient, and spring stiffness coefficient, respectively, $f_{IL}(t)$ denotes the van der Waals attraction/ repulsion force (i.e., the interaction forces) for lumped-model which is explicitly defined in the following form [11]:

$$f_{IL} = \frac{Dk}{(z_0 - x)^2} - \frac{\sigma^6 Dk}{30(z_0 - x)^8} \qquad (2)$$

where z_0 represents the distance from the fixed base frame coordinate to the sample, σ denotes the molecular diameter, and the model parameter D is defined as $D = \frac{A_H R}{6k}$ where A_H denotes the Hamaker constant, and R represents the cantilever tip radius. Furthermore, the total cantilever tip displacement is constrained by the following inequality [11].

$$z - x \geq R \qquad (3)$$

The cantilever is driven through $d(t)$ as:

$$d(t) = A\sin(\omega t) \qquad (4)$$

where A is the drive amplitude and ω is the drive frequency. If $d(t)$ is replaced in cantilever-sample interaction equation (1), it yields:

$$\ddot{x}(t) = -\omega_0^2 x_1 + \frac{D\omega_0^2}{(z_0 - x)^2} - \frac{\sigma^6 D\omega_0^2}{30(z_0 - x)^8} + \omega_0^2 A\sin(\omega t) + A\omega\frac{b}{m_e}\cos(\omega t) - \frac{b}{m_e}\dot{x}_1 \qquad (5)$$

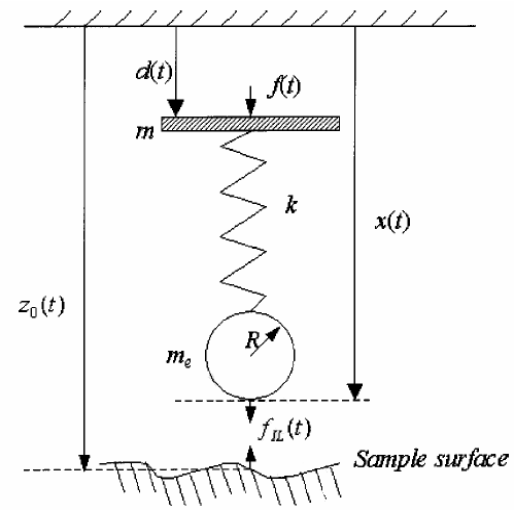

Fig. 2. Lumped-parameters model of the AFM system (from [1]).

We intend to use the Melnikov method in order to determine the region possible for chaos. It must be noted that this method was used in [14], but the model was simpler and different from the one used here. To achieve this goal initially, the model is considered as simple Hamiltonian system and omitted terms will then be added as perturbation terms. If we exert this assumption on the system, the Hamiltonian of the system and the equations of motion in state space form will be in the form:

$$x_1 = x\ ,\ x_2 = \dot{x} \qquad (6)$$

$$H = \frac{1}{2}x_2^2 + \frac{1}{2}\omega_0^2 x_1^2 - \frac{D\omega_0^2}{(z_0 - x_1)} + \frac{\sigma^6 D\omega_0^2}{210(z_0 - x_1)^7} \qquad (7)$$

$$\dot{x}_1 = x_2$$

$$\dot{x}_2 = -\omega_0^2 x_1 + \frac{D\omega_0^2}{(z_0 - x_1)^2} - \frac{\sigma^6 D\omega_0^2}{30(z_0 - x_1)^8} \qquad (8)$$

The equilibrium points of this system are simply:

$$x_2 = 0$$

$$\frac{D\omega_0^2}{(z_0 - x_1)^2} - \frac{\sigma^6 D\omega_0^2}{210(z_0 - x_1)^7} = \omega_0^2 x_1 \qquad (9)$$

Since the second term in left side of the second equation in (7) is negligible relative to the first term, we can use the results in [14] with the critical value of $z_s = \frac{3}{2}(2D)^{1/3}$. Hence, the equilibrium points obtained here can be classified in the following categories:

If $z_0 \geq z_s$, there are three equilibrium points of :

$$0 < x_{11} \leq \frac{z_s}{3} \quad , \quad \frac{z_s}{3} \leq x_{12} < z_0 \quad , \ x_{13} \cong z_0 \qquad (10)$$

If $z_0 < z_s$, there is one equilibrium point of $x_{11} \cong z_0$. Figure 3 depicts the loci of these (equilibrium) points.

In this paper, we consider only the case for which $z_0 \geq z_s$ (i.e., only non-contact operation of AFM) which includes three equilibrium points. Notice, for $z_0 < z_s$ the sample will attract the tip into contact.

In order to facilitate the study, the following relations are introduced.

$$\tau = \omega_0 t,\ y_1 = \frac{x_1}{z_s},\ y_2 = \frac{x_2}{\omega_0 z_s},\ \alpha = \frac{z_0}{z_s},\ \hat{\sigma} = \frac{\sigma}{z_s},\ d = \frac{4}{27} \tag{11}$$

Hence, the system equations (8) reduce to:

$$y_1' = y_2$$

$$y_2' = -y_1 + \frac{d}{(\alpha - y_1)^2} - \frac{\hat{\sigma}^6 d}{30(\alpha - y_1)^8} \tag{12}$$

where the prime denotes the derivative with respect to special variable τ defined in (11).

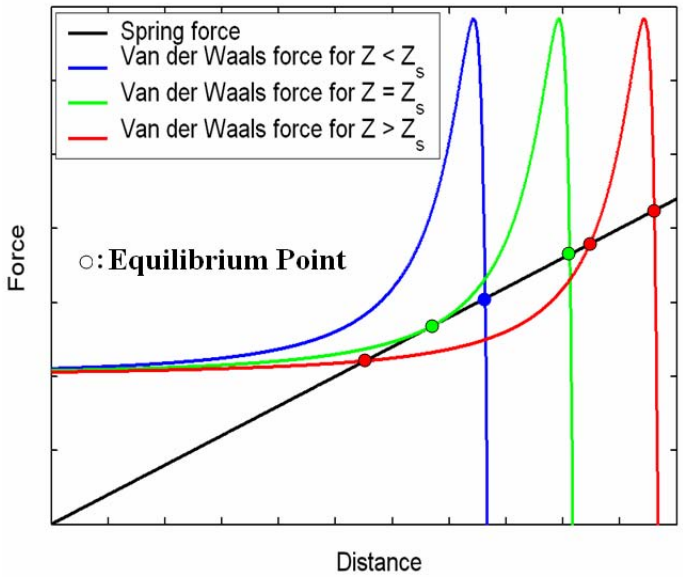

Fig. 3 Root locus plot of the system equilibrium points.

PHASE PORTRAIT ANALYSIS

The behavior of the system near the equilibrium points can be revealed by linearizing the system as given by.

$$\begin{pmatrix} \dot{x}_1 \\ \dot{x}_2 \end{pmatrix} = \begin{bmatrix} 0 & 1 \\ -1 + \frac{2d}{(\alpha - x_{1i})^3} - \frac{8\hat{\sigma}^6 d}{(\alpha - x_{1i})^9} & 0 \end{bmatrix} \begin{pmatrix} x_1 \\ x_2 \end{pmatrix} \quad 1 \leq i \leq 3 \tag{13}$$

The eigenvalues of the linearized system are purely imaginary at x_{11} and x_{13}, while they are complex conjugates at x_{12}. Thus, the equilibrium point x_{12} is a saddle point. Based on the center manifold theorem nothing can be concluded about the stability nature of a point by linearizing when the points are pure imaginary. To discover the nature of the system behavior near x_{11} and x_{13}, the phase portrait of the system can be drawn as shown in Figure 4.

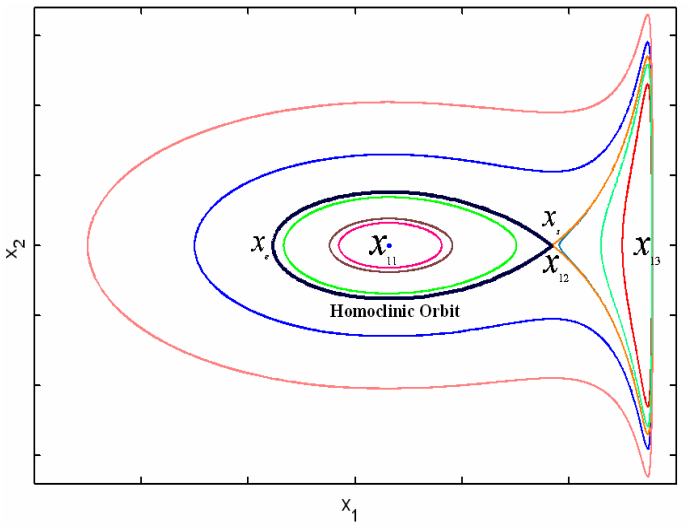

Fig. 4 Phase Portrait of the original system (12).

The actual system is not Hamiltonian, since it is damped by the surrounding air and also by the cantilever structure, as well as it is excited at the base. The actual system equation in the non-dimensional state space can be represented as:

$$\dot{\mathbf{x}} = \mathbf{f}(\mathbf{x}) + \varepsilon\, \mathbf{g}(\mathbf{x}, t) \tag{14}$$

where:

$$\mathbf{f}(\mathbf{x}) = \begin{pmatrix} x_2 \\ -x_1 + \frac{d}{(\alpha - x_1)^2} - \frac{\hat{\sigma}^6 d}{30(\alpha - x_1)^8} \end{pmatrix} \tag{15}$$

$$\mathbf{g}(\mathbf{x}) = \mathbf{g}(x_2, t) = \begin{pmatrix} 0 \\ q\sin(\Omega t) + q\, p\, \Omega \cos(\Omega t) - p x_2 \end{pmatrix} \tag{16}$$

$$p = \frac{b}{me\,\omega_0^2},\ q = \frac{A}{z_s},\ \Omega = \frac{\omega}{\omega_0} \tag{17}$$

In (14), $\mathbf{g}$ is a periodic function of period $\frac{2\pi}{\Omega}$. Note that this system can be written as an autonomous system in $\Re^3$ by defining $\dot{x}_3 = \dot{\phi} = \Omega$.

The Melnikov function, $M(t_0)$, is then defined as:

$$M(t_0) = \int_{-\infty}^{\infty} e^{-\int_{t_0}^{t} \nabla \cdot \mathbf{f}(\gamma_0(s))\, ds}\, \mathbf{f}(\gamma_0(t)) \wedge \mathbf{g}(\gamma_0(t), t + t_0)\, dt \tag{18}$$

where the wedge product of two vectors u and v $\in \Re^2$ is defined as $u \wedge v = u_1 v_2 - v_1 u_2$. Note that the Melnikov function $M(t_0)$ is proportional to the derivative of the Poincare map with respect to the parameter ε in an interior neighborhood of the separatrix cycle Γ_0 (or in a neighborhood of a cycle).

$M(t_0)$ is a measure of separation of the stable and unstable manifolds of the Poincare map P_ε. In the other hand, the Melnikov function is a signed measure of the distance between the stable and unstable manifolds for the perturbed system. Hence, The intersection of manifolds indicates the possibility of the presence of chaos [17, 18].

Along this line, an attempt is made here to determine $M(t_0)$ in the AFM system as a function of system parameters:

$$\begin{aligned} M(t_0) &= \int_{-\infty}^{\infty} x_{2h}(t))\, g_2(x_{1h}(t), x_{2h}(t), \phi(t+t_0))\, dt \\ &= \int_{-\infty}^{\infty} x_{2h}(t)\ (q\sin(\Omega(t+t_0)) + q\, p\Omega\cos(\Omega(t+t_0)) - p x_2) dt \\ &= -2p\int_0^{\infty} x_{2h}^2(t)\, dt + q\int_{-\infty}^{\infty} x_{2h}(t)\ \sin(\Omega(t+t_0))dt \\ &+ q\, p\Omega\int_{-\infty}^{\infty} x_{2h}(t)\cos(\Omega(t+t_0))dt \end{aligned} \tag{19}$$

with

$$\int_{-\infty}^{\infty} x_{2h}(t)\ \sin(\Omega(t+t_0))dt = 2\cos(\Omega t_0)\int_0^{\infty} x_{2h}(t)\ \sin(\Omega t)dt \tag{20}$$

$$\int_{-\infty}^{\infty} x_{2h}(t)\ \cos(\Omega(t+t_0))dt = -2\sin(\Omega t_0)\int_0^{\infty} x_{2h}(t)\ \sin(\Omega t)dt \tag{21}$$

where $x_{1h}(t)$ and $x_{2h}(t)$ are the homoclinic solutions [14]. In obtaining the above equalities, we have used the fact that $x_{2h}(t)$ is an odd function of time. Hence, we have:

$$M(t_0) = -2p\, S(\alpha) - 2q\sqrt{1+p^2\Omega^2}\ \sin(\Omega t_0 - \theta)\, N(\alpha,\Omega) \tag{22}$$

Where

$$\begin{aligned} &\theta = \arctan(\frac{1}{p\Omega})\ ,\ S(\alpha) = \int_0^{\infty} x_{2h}^2(t)\, dt\,, \\ &N(\alpha,\Omega) = \int_0^{\infty} x_{2h}(t)\sin(\Omega t)\, dt\,,\ R_a = \frac{S(\alpha)}{N(\alpha,\Omega)} \end{aligned} \tag{23}$$

The Melnikov function will have zeros if and only if $q\sqrt{\frac{1}{p^2}+\Omega^2} \geq R_a$. If this condition is not satisfied, then $M(t_0)$ has no zeros.

In order to simplify the procedure of computing $S(\alpha)$ and $N(\alpha,\Omega)$, the integration variable is changed to x_1 as:

$$S(\alpha) = \int_0^{\infty} x_{2h}^2(t)\, dt = \int_{x_e}^{x_s} x_{2h}(x_1)\, dx_1 = \int_{x_e}^{x_s} (x_s - x_1)\sqrt{\frac{x_1 - x_e}{\alpha - x_1}}\ dx_1 \tag{24}$$

$$N(\alpha,\Omega) = \int_0^{\infty} x_{2h}(t)\sin(\Omega t)\, dt =$$

$$\int_{x_e}^{x_s} \sin(\Omega(-\arcsin(\frac{x_1 + x_s - \alpha}{x_s}) - \sqrt{\frac{\alpha - x_s}{3x_s - \alpha}}\ \ln(G) - \frac{\pi}{2}))\, dx_1 \tag{25}$$

The region R_a can now be computed numerically for different values of $\alpha > 1$, Ω around 1. The results are plotted as shown in Figure 5.

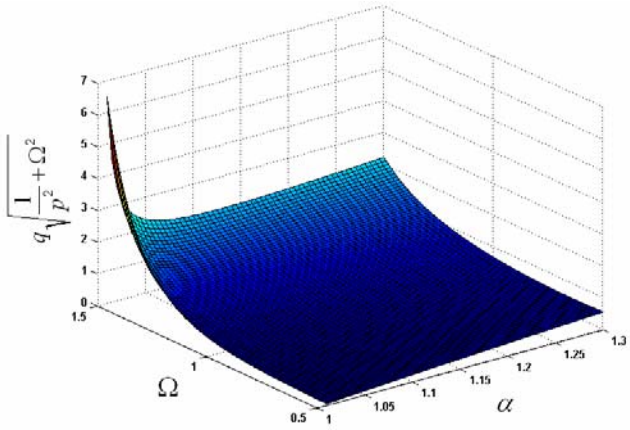

Fig. 5 R_a Surface where above the surface is the region where chaos may exist in the system. The region below the surface is the region where only periodic motions exist in the system.

Intersection of the stable and the unstable manifolds occurs for points which lie above the surface plotted in Figure 5. As α increases, the system tends to the spring-mass-damper system behavior which does not exhibit chaotic motion when it is perturbed by the harmonically exciting spring base. In this case, the exact trajectories of system can be found analytically. When α is close enough to 1, the possibility of intersection of stable and unstable manifolds increases. This means small perturbations may create chaotic motions.

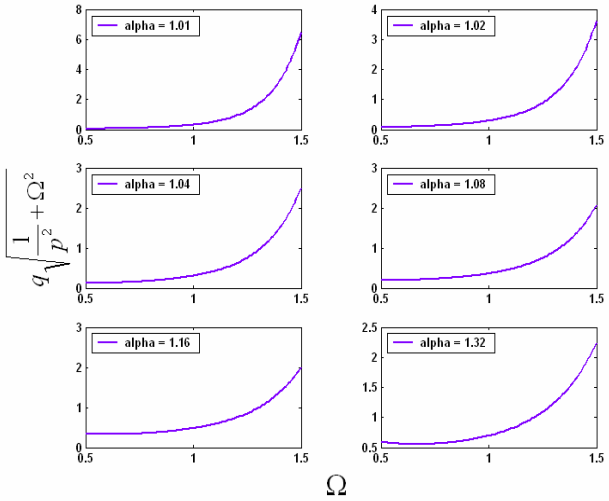

Fig. 6 The region above the curves is the region where chaos may exist.

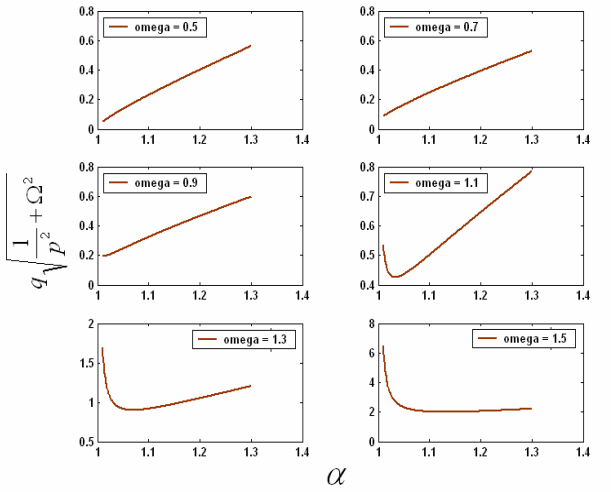

Fig. 7 The region above the curves is the region where chaos may exist.

Figures 6 and 7 depict dependence of R_a on the changes of α and Ω. As Ω increases, both R_a and $\sqrt{\frac{1}{p^2}+\Omega^2}$ increase. This means that, with fixed amplitude (q) and sample position (α), increasing the excitation frequency may decrease or increase the possibility of chaos depending on the values of physical parameters of the system p. All in all, the Melnikov theory determine the region that chaotic invariant sets exist, but the presence of a chaotic invariant set does not always imply the existence of a chaotic attractor. Therefore, in order to prove the theoretical results, numerical analysis should be focused on finding chaotic attractors in the region described above. To this end, a specific system with physical parameters suitable for chaos is considered where we examine the presence of chaos by using different tools.

CHAOS DETECTION

Let us consider the system in (14), where the parameters have been set as follows:

$$\Omega = 1.1 \ , \ \alpha = 1.2 \ , \ \widehat{\sigma} = 0.3 \ , \ p = 0.02 \tag{26}$$

For these parameter values, the critical value obtained from the Melnikov function method is $q_{Melnikov} = 0.01292$. Since $\alpha \geq 1$, the unperturbed system ($\varepsilon = 0$) shows the presence of three equilibrium points. The system shows the periodic motions for $q \leq q_{Melnikov}$. In the following, several methods of chaotic behavior detection are presented.

Period Doubling Route to Chaos:

If chaos theory is the study of the pathways from simple to complex dynamics, then period doubling must be considered one of the principal routes to chaotic behavior in physical systems with nonlinearities. Periodic doubling is a phenomenon in which the period of repetition of a cyclic dynamic process doubles with the change of some control parameter, and continues to double at successively closer parameter values until the period is so long and becomes practically aperiodic [18]. In system considered here, by increasing q the phenomena of period doubling will appear as shown in Figure 8.

Poincare Maps:

Poincare maps are one of the principal ways of recognizing chaotic vibrations in low-degree-of-freedom problems. Chaotic phase-plane trajectories can often be unraveled using the Poincare map by taking a set of pictures for different phases as shown in Figure 9. This is tantamount to sweeping the Poincare plane in three dimensional phase space with respect to variable ϕ. While one Poincare map can be used to expose the fractal nature of the attractor, a complete set of maps varying from 0 to 2π is sometimes needed to obtain a complete picture of the attractor on which the motion is riding. Since our AFM system considered here does not have sufficient damping, then the chaotic attractor tends to approximately uniformly fill up a section of phase space and the Cantor set structure, which is characteristic of strange attractors, is not completely evident [19].

Fourier Spectrum:

This is by far the most popular measure mainly because the idea of decomposing a nonperiodic signal into a set of sinusoidal or harmonic signals is widely known among scientists and engineers. One detecting chaotic vibration tool is the appearance of a broad spectrum of frequencies in the output when the input is a single-frequency harmonic motion. When three or more incommensurate frequencies are present, one may not see a nice closed curve in the Poincare map and the Fourier spectrum should be used. The difference between chaotic and quasi-periodic motion can also be detected by taking the Fourier spectrum of the signal. A quasi-periodic motion will have a few well-pronounced peaks. The assumption made in this method is that the periodic or nonperiodic signal can be represented as a synthesis of sine or cosine signals:

$$f(t) = \frac{1}{2\pi}\int_{\Gamma} F(\omega) e^{i\omega t} d\omega \tag{27}$$

When the motion is periodic or quasi-periodic, $|F(\omega)|$ shows a set of narrow spikes or lines indicating that the signal can be represented by a discrete set of harmonic functions $\left\{e^{\pm i\omega_k t}\right\}$, where $k = 1,2,\ldots,n$. Near the onset of chaos, however, a continuous distribution of frequency appears (see Figure 10), and in the fully chaotic regime the continuous spectrum may dominate the discrete spikes. Given a set of data sampled at discrete even time intervals $\left\{f(t_k) = f_0, f_1, f_2, \ldots, f_k, \ldots, f_N\right\}$, the discrete time fast Fourier transform is defined as:

$$T(m) = \sum_{k=1}^{N} f(k) e^{-2\pi i(k-1)(m-1)/N} \tag{28}$$

where k and m are integers [19]. As seen from Figure 10, the Fourier spectrum of the considered system shows a distribution of frequencies that exists in the signal, confirming the presence of chaos.

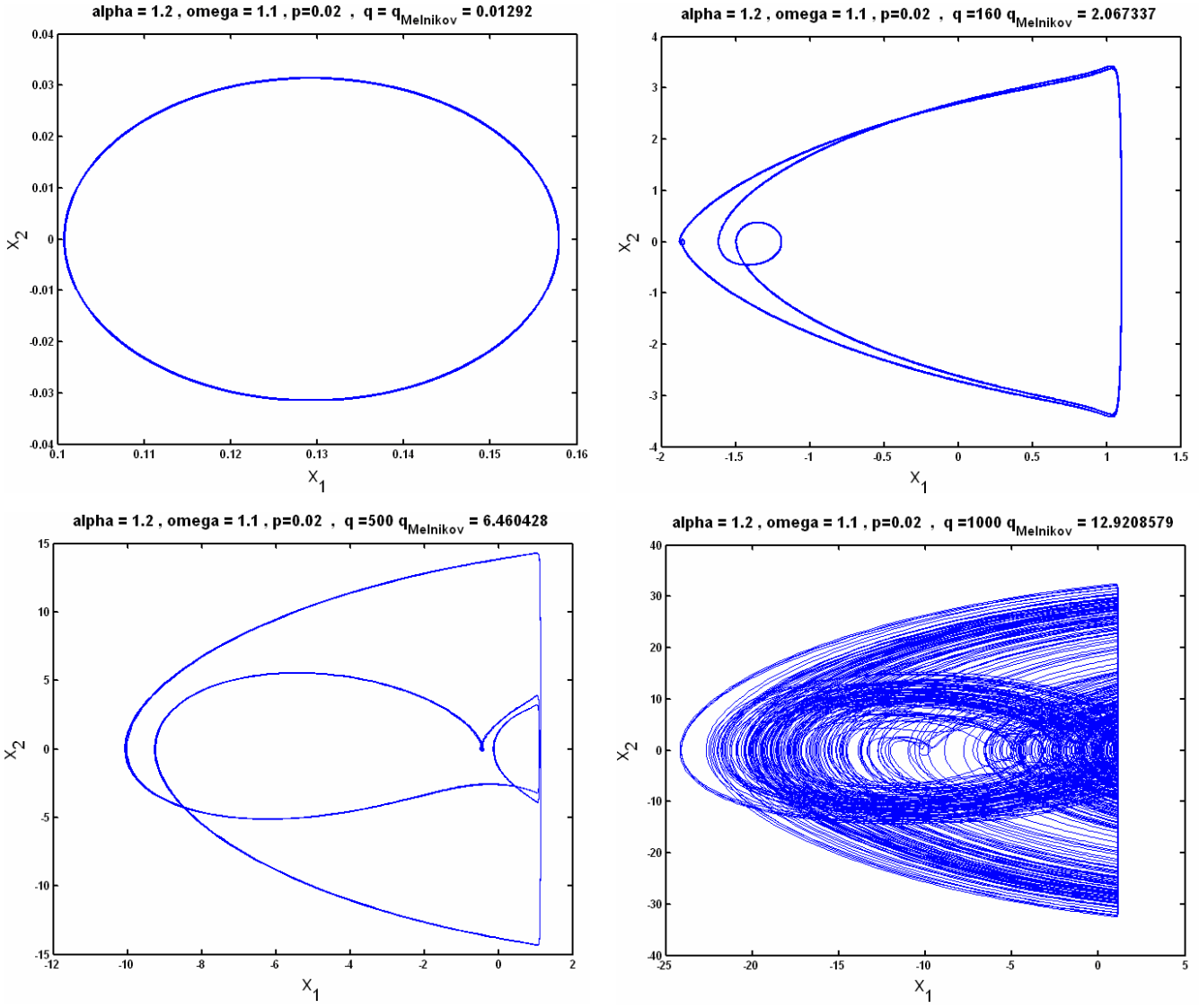

Fig. 8 The phase portrait of perturbed system for different values of drive amplitude.

Lyapunov Exponents:

Loss of Information about initial conditions is another property of a chaotic system. The Lyapunov exponent test measures the sensitivity of the system to changes in initial conditions. Lyapunov exponents give a means of describing the stretching and contracting characteristics of attractors and other invariant sets [20]. Conceptually, one could imagine a small ball of initial conditions in phase space, while looking at its deformation into an ellipsoid under the dynamics of the system. If d is the maximum length of ellipsoid and d_0 is the initial size of the initial condition sphere, the Lyapunov exponent λ is interpreted by the below equation [19]:

$$d = d_0 2^{\lambda(t-t_0)} \tag{29}$$

(30)

One measurement, however, is not sufficient, and the calculation must be averaged over different regions of phase space. This average can be represented by:

$$\lambda = \lim_{t\to\infty} \frac{1}{N} \sum_{1}^{N} \frac{1}{(t_i - t_{0i})} \log_2\left(\frac{d_i}{d_{0i}}\right) \tag{31}$$

Then,

$\lambda > 0$: Chaotic motion

$\lambda \le 0$: Regular motion

In the system considered here with $q = 12.921$, the dominant Lyapunov exponent can be evaluated as: $\lambda_{\max} = 0.035$ which is an indication of chaotic behavior in the system.

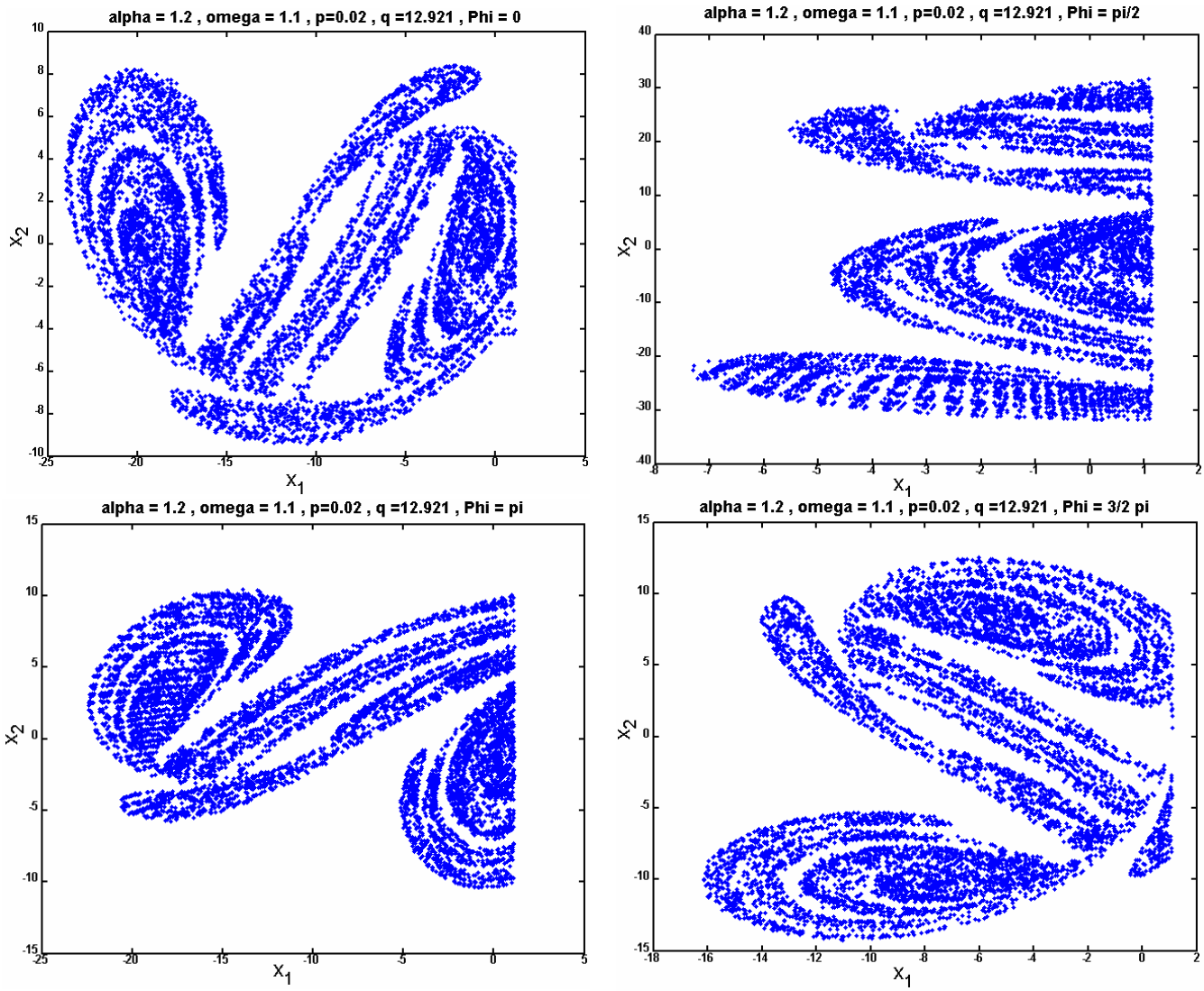

Fig. 9 The Poincare Maps for different values of phase ϕ.

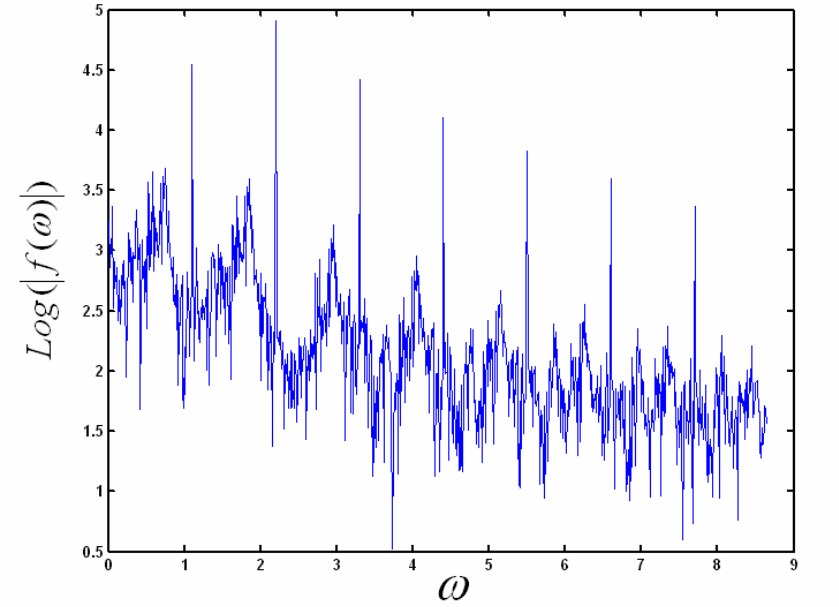

Fig. 10 The Fourier spectrum.

CONCLUSIONS

A lumped-parameters model for an AFM system modeled as a cantilever beam was utilized to determine the dynamical behavior of the sample-tip interaction. The presence of chaotic invariant sets is theoretically proved by using the Melnikov method, which reveals the region in the space of physical parameters where chaotic motion is possible. The existence of such chaotic invariant sets predicted by Melnikov theory was then numerically verified through several methods including Poincare maps, Lyapunov exponents, autocorrelation function, Fourier transform. As expected, the chaotic attractors lie in a subset of the invariant set predicted by Melnikov theory.

REFERENCES

[1] Jalili, N. and Laxminarayana, K., 2004, "A Review of Atomic Force Microscopy Imaging Systems: Application to Molecular Metrology and Biological Sciences", *International Journal of Mechatronics,* **14** (8), pp. 907-945.

[2] Goeken, M. and Kempf, M., 1999, ''Microstructural Properties of Super alloys Investigated by Nanoindentations in an Atomic Force Microscope,'' *ActaMater.*, **47**(3), pp. 1043–1052.

[3] Kempf, M., Go¨ken, M. and Vehoff, H., 1998, ''Nanohardness Measurements for Studying Local Mechanical Properties of Metals,'' *Appl. Phys. A: Mater. Sci. Process.*, **66**, pp. S843–S846.

[4] Nagashima, N., Matsuoka, S. and Miyahara, K., 1996, ''Nanoscopic Hardness Measurement by Atomic Force Microscope,'' *JSME International Journal, Series A: Mechanics and Material Engineering*, **39**(3), pp. 456–462.

[5] Gahlin, R. and Jacobson, S., 1998, ''Novel Method to Map and Quantify Wear on a Micro-Scale,'' *Wear*, **222**(2), pp. 93–102.

[6] Miyahara, K., Nagashima, N., Ohmura, T. and Matsuoka, S., 1999, ''Evaluation of Mechanical Properties in Nanometer Scale Using AFM-Based Nanoindentation Tester,'' *Nanostruct. Mater.*, **12**(5), pp. 1049–1052.

[7] Sundararajan, S. and Bhushan, B., 2001, ''Development of a Continuous Microscratch Technique in an Atomic Force Microscope and Its Application to Study Scratch Resistance of Ultrathin Hard Amorphous Carbon Coatings,'' *J. Mater. Res.*, **16**(2), pp. 437–445.

[8] Chen, W., Ahmed, H. and Nakazoto, K., 1995, ''Coulomb Blockade at 77 K in Nanoscale Metallic Islands in a Lateral Nanostructure,'' *Appl. Phys. Lett.*, **66**(24), p. 3383.

[9] Klein, D. L., McEuen, P. L., Katari, J. E. B., Roth, R. and Alivisatos, A. P., 1996, ''Approach to Electrical Studies of Single Nanocrystals,'' *Appl. Phys. Lett.*, **68**(18), p. 2574.

[10] Bezryadin, A., Dekker, C. and Schmid, G., 1997, ''Electrostatic Trapping of Single Conducting Nanoparticles Between Nanoelectrodes,'' *Appl. Phys. Lett.*, **71**(9), pp. 1273–1275.

[11] Jalili, N., Dadfarnia, M. and Dawson, D. M., 2004 "A Fresh Insight into the Microcantilever-Sample Interaction Problem in Non-Contact Atomic Force Microscopy", *ASME Journal of Dynamic Systems, Measurements and Control*, **126** (2), pp. 327-335.

[12] Sebastian, A., Salapaka, M., Chen, D. and Cleveland, J., 1999, "Harmonic Analysis Based Modeling of Tapping-Mode AFM," *Proceedings of the American Control Conference*, San Diego, CA, pp. 232-236.

[13] Basso, M., Giarre, L., Dahleh, M. and Mezic, I., 1998, ''Numerical Analysis of Complex Dynamics in Atomic Force Microscopes,'' *Proceedings of the IEEE Conference on Control Applications*, Trieste, Italy, pp. 1026–1030.

[14] Ashhab, M., Salapaka, M., Dahleh, M. and Mezic, I., 1999, ''Dynamical Analysis and Control of Microcantilevers,'' *Automatica*, **35**, pp. 1663–1670.

[15] Hsu, S. and Fu, L. 1999, ''Robust Output High-Gain Feedback Controllers for the Atomic Force Microscope Under High Data Sampling Rate,'' *Proceedings of the IEEE International Conference on Control Applications*, Kohala Coast-Island, HI, pp. 1626–1631.

[16] Fang,Y., Feemster, M. G., Dawson, D. M. Jalili, N., "Nonlinear Control Techniques For the Atomic Force Microscope System", *Proceedings of the 2002 ASME International Mechanical Engineering Congress and Exposition,* November 2002, New Orleans, LA, USA.

[17] Perko, L., "Differential Equations and Dynamical Systems", Springer-Verlag (NY), 1991.

[18] Wiggins, S., "Introduction to Applied Nonlinear Dynamical Systems and Chaos", Springer-Verlag (NY), 1990

[19] Moon, F. C., "Chaotic and Fractal Dynamics", John Wiley & Sons, Inc., (NY), 1992

[20] Ott, E., "Chaos in Dynamical Systems", Cambridge University Press, 2002.